Investigation of resonances in the $\Sigma(1/2^-)$ system based on the chiral quark model*

Yu Yao (姚宇)[1] Xuejie Liu (刘雪杰)[2] Xiaoyun Chen (陈晓云)[3] Yuheng Wu (吴雨衡)[1] Jialun Ping (平加伦)[4]
Yue Tan (谭悦)[1†] Qi Huang (黄琦)[4‡]

[1]Department of Physics, Yancheng Institute of Technology, Yancheng 224000, China
[2]Department of Physics, Henan Normal University, Xinxiang 453007, China
[3]College of Science, Jinling Institute of Technology, Nanjing 211169, China
[4]Department of Physics, Nanjing Normal University, Nanjing 210023, China

Abstract: In this work, we investigate the resonance structures in the $\Sigma(1/2^-)$ system from both three-quark and five-quark perspectives within the framework of the chiral quark model. An accurate few-body computational approach, the Gaussian expansion method, is employed to construct the orbital wave functions of multiquark states. To reduce the model dependence on parameters, we fit two sets of parameters to check the stability of the results. The calculations show that our results remain stable despite changes in the parameters. In the three-quark calculations, two $\Sigma(1/2^-)$ states are obtained with energies around 1.8 GeV, which are good candidates for the experimentally observed $\Sigma(1750)$ and $\Sigma(1900)$. In the five-quark configuration, several stable resonance states are identified, including $\Sigma\pi$, $N\bar{K}$, and $N\bar{K}^*$. These resonance states survive the channel-coupling calculations under the complex-scaling framework and manifest as stable structures. Our results support the existence of a two-pole structure for the $\Sigma(1/2^-)$ system, predominantly composed of $\Sigma\pi$ and $N\bar{K}$ configurations, analogous to the well-known $\Lambda(1380)$-$\Lambda(1405)$ ($\Sigma\pi$-$N\bar{K}$) system. On the other hand, although the energy of the $N\bar{K}^*$ configuration is close to that of $\Sigma(1750)$ and $\Sigma(1900)$, the obtained width is not consistent with the experimental values. This suggests that the $N\bar{K}^*$ state needs to mix with three-quark components to better explain the experimental $\Sigma(1750)$ and $\Sigma(1900)$ states. According to our decay width calculations, the predicted two resonance states are primarily composed of $\Sigma\pi$ and $N\bar{K}$, with their main decay channel being $\Lambda\pi$. Therefore, we encourage experimental groups to search for the predicted two-pole structure of the $\Sigma(1/2^-)$ system in the invariant mass spectrum of $\Lambda\pi$.

Keywords: quark model, resonances, hardon spectrum, complex-scaling method

DOI: 10.1088/1674-1137/ae18af **CSTR:** 32044.14.ChinesePhysicsC.50023109

I. INTRODUCTION

The search for exotic states has long been a hot topic in hadron physics, with multiquark configurations playing a crucial role in their interpretation. In the framework of the traditional quark model, baryons are described as three-quark states and mesons as quark-antiquark pairs. This has been remarkably successful in describing a large number of ground-state hadrons [1, 2]; however, it faces significant challenges in explaining certain excited hadrons such as the $X(3872)$ [3] and $\Lambda(1405)$ [4]. It is now widely believed that many excited hadrons may have substantial multiquark components in their internal structure. Understanding interactions among multiquark systems and revealing their underlying structure is essential for deepening our comprehension of quantum chromodynamics (QCD).

Among the excited baryons, the resonance structures in the $\Sigma(1/2^-)$ system have attracted sustained interest. Experimentally, four $\Sigma(1/2^-)$ states were observed to date [5], namely, $\Sigma(1620)$, $\Sigma(1750)$, $\Sigma(1900)$, and $\Sigma(2110)$. However, various theoretical studies [6−11] suggested the possible existence of a stable structure in the mass range of 1.3−1.4 GeV. In Ref. [6], the authors construc-

Received 12 June 2025; Accepted 29 October 2025; Accepted manuscript online 30 October 2025

* Supported partly by the National Science Foundation of China (12205249, 12305087). Yue Tan is supported by the Funding for School-Level Research Projects of Yancheng Institute of Technology (xjr2022039) and the Qinglan Project Fund of Jiangsu Province. Qi Huang is supported by the Start-up Funds of Nanjing Normal University (184080H201B20)

† E-mail: tanyue@ycit.edu.cn (Corresponding author)
‡ E-mail: huangqi@njnu.edu.cn (Corresponding author)

ted a diquark picture for the pentaquark with $J^P = 1/2^-$ and predicted the lowest mass of the $\Sigma(1/2^-)$ state to be ~1.36 GeV, while the corresponding lowest $\Lambda(1/2^-)$ state lies at 1.44 GeV. This result is consistent with the observed $\Lambda(1405)$. Using the effective Lagrangian approach, Ref. [7] investigated the $K^- p \to \Lambda\pi^-\pi^+$ reaction near the $\Lambda^*(1520)$ peak and found evidence for a new resonance around 1.38 GeV. This result was later confirmed in Ref. [8] through a re-examination of older $K^- p \to \Lambda\pi^-\pi^+$ data, which further suggested that the width of this resonance could be larger than previously estimated. More recently, Ref. [9] explored the role of triangle singularities in the process $J/\psi \to \Lambda\bar{\Lambda}\pi$. The triangle singularity plays a significant role in shaping the $\Lambda\pi$ invariant mass spectrum, leading to the appearance of a resonance-like structure around 1.4 GeV. Similarly, within the triangle singularity framework and using an effective Lagrangian approach, Ref. [11] investigated resonance production in the reaction $\Lambda_c^+ \to \gamma\pi^+\Lambda$, which predicts a resonance near 1.38 GeV. Σ baryons, as isospin partners of the Λ states, exhibit a similar spectral structure. Figure 1 shows that the energy of the $\Sigma(1/2^+)$ state is ~76 MeV higher than that of the $\Lambda(1/2^+)$ state. In the $J^P = 1/2^-$ sector, if we disregard the experimentally uncertain $\Sigma(1620)$ state (which currently has only a one-star rating), a parallel pattern can be observed: $\Sigma(1750)$ and $\Sigma(1900)$ correspond to $\Lambda(1670)$ and $\Lambda(1800)$, respectively. Based on this correspondence, the well-established $\Lambda(1405)$ and tentative $\Lambda(1380)$ (though the latter lacks strong experimental confirmation) would naturally imply the existence of a Σ resonance in the mass range of 1.3−1.4 GeV.

It is widely accepted that the $\Lambda(1405)$ and tentative $\Lambda(1380)$ arise from a two-pole structure [12−15] generated by the coupled-channel interaction between the $N\bar{K}$ and $\Sigma\pi$ channels. That is, under strong channel coupling effects, both $N\bar{K}$ and $\Sigma\pi$ components remain dynamically stable. In this study, within the framework of the chiral quark model and with the help of a high-precision few-body method, the Gaussian expansion method (GEM) first calculates the energy of the $\Sigma(1/2^-)$ system in the three-quark configuration. Then, we focus on the five-quark picture, where we perform bound-state calculations for the $\Sigma(1/2^-)$ system in various physical channels, whic includes $N\bar{K}$, $\Sigma\pi$, and others. Subsequently, the complex-scaling method, which is a powerful tool for identifying resonance states, is employed for examining the stability of the resonances found in bound-state calculations. In our analysis, the effects of channel coupling are thoroughly considered as we couple the obtained states to all relevant scattering channels.

The remainder of this paper is organized as follows: Sec. II provides a brief description of the quark model, construction of wave functions, and overview of the complex-scaling method. Our numerical results and related discussions are presented in Sec. III. Finally, a summary is given in Sec. IV.

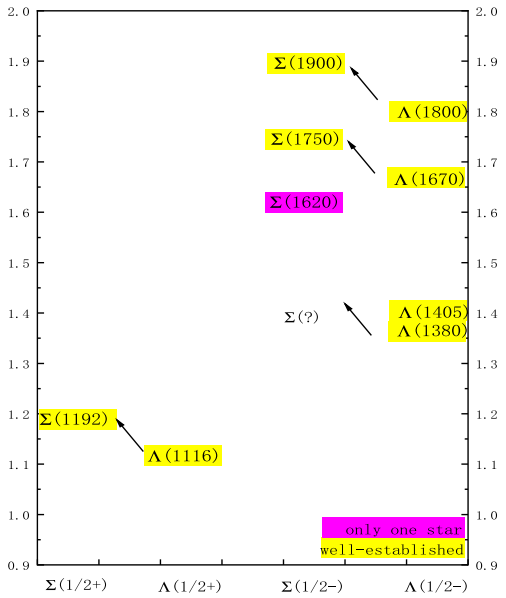

Fig. 1. (color online) Comparison of energy levels between Σ and Λ baryons.

II. MODEL SETUP

A. Chiral quark model

In this study, the chiral quark model is employed to investigate the $\Sigma(1/2^-)$ system. The chiral quark model [16−18] has become one of the most widely used approaches in hadron spectroscopy, hadron-hadron interactions, and study of multiquark states because of its successful explanation of a large amount of experimental data. In this model, in addition to one-gluon exchange, the massive constituent quarks interact with each other via the Goldstone boson exchange. Furthermore, color confinement and meson exchange are incorporated into the model. The Hamiltonian of the chiral quark model is expressed as

$$H = \sum_{i=1}^{n}\left(m_i + \frac{\vec{p}_i^{\,2}}{2m_i}\right) - T_c + \sum_{i<j=1}^{n} V(r_{ij}), \tag{1}$$

where m_i, $\vec{p}_i$, T_c, and $V(r_{ij})$ represent the quark mass, quark momentum, center-of-mass kinetic energy of the quark system, and potential term, respectively. In the Jacobi coordinate system for a three-quark system, the kinetic term $\sum_{i=1}^{n}\left(m_i + \frac{\vec{p}_i^{\,2}}{2m_i}\right) - T_c$ can be reduced to

$$\frac{\vec{p}_{12}^{\,2}}{2\mu_{12}} + \frac{\vec{p}_{12,3}^{\,2}}{2\mu_{12,3}}, \tag{2}$$

and for a five-quark system, it can be reduced to

$$\frac{\vec{p}_{12}^2}{2\mu_{12}}+\frac{\vec{p}_{12,3}^2}{2\mu_{12,3}}+\frac{\vec{p}_{45}^2}{2\mu_{45}}+\frac{\vec{p}_{123,45}^2}{2\mu_{123,45}}. \tag{3}$$

We are studying light hadronic states (with quark constituents u, d, and s), and therefore, the chiral potential, including the Goldstone boson exchanges (π, η, K) and scalar meson exchanges (a_0, f_0, κ, σ), play a crucial role. Among these, the scalar meson exchanges are important for resolving the $\rho-\omega$ mass inversion problem [19]. The interaction potentials are

$$\begin{aligned}
V_\pi(r_{ij}) &= \frac{g_{\rm ch}^2}{4\pi}\frac{m_\pi^2}{3m_im_j}\frac{\Lambda_\pi^2 m_\pi}{\Lambda_\pi^2-m_\pi^2}\hat{S}_i\cdot\hat{S}_j\sum_{a=1}^{3}\lambda_i^a\lambda_j^a \\
&\quad\times\left[Y(m_\pi r_{ij})-\frac{\Lambda_\pi^3}{m_\pi^3}Y(\Lambda_\pi r_{ij})\right], \\
V_K(r_{ij}) &= \frac{g_{\rm ch}^2}{4\pi}\frac{m_K^2}{3m_im_j}\frac{\Lambda_K^2 m_K}{\Lambda_K^2-m_K^2}\hat{S}_i\cdot\hat{S}_j\sum_{a=1}^{3}\lambda_i^a\lambda_j^a \\
&\quad\times\left[Y(m_K r_{ij})-\frac{\Lambda_K^3}{m_K^3}Y(\Lambda_K r_{ij})\right], \\
V_\eta(r_{ij}) &= \frac{g_{\rm ch}^2}{4\pi}\frac{m_\eta^2}{3m_im_j}\frac{\Lambda_\eta^2 m_\eta}{\Lambda_\eta^2-m_\eta^2}\hat{S}_i\cdot\hat{S}_j\left(\lambda_i^8\lambda_j^8\cos\theta_P\right. \\
&\quad\left.-\lambda_i^0\lambda_j^0\sin\theta_P\right)\left[Y(m_\eta r_{ij})-\frac{\Lambda_\eta^3}{m_\eta^3}Y(\Lambda_\eta r_{ij})\right], \\
V_s(r_{ij}) &= v_\sigma(\mathbf{r}_{ij})\lambda_i^0\lambda_j^0+v_{a_0}(\mathbf{r}_{ij})\sum_{a=1}^{3}\lambda_i^a\lambda_j^a \\
&\quad v_k(\mathbf{r}_{ij})\sum_{a=4}^{7}\lambda_i^a\lambda_j^a+v_{f_0}(\mathbf{r}_{ij})\lambda_i^8\lambda_j^8, s=a_0,f_0,\kappa,\sigma \\
v_s &= -\frac{g_{\rm ch}^2}{4\pi}\frac{\Lambda_s^2}{\Lambda_s^2-m_s^2}m_s\left[Y(m_s r_{ij})-\frac{\Lambda_s}{m_s}Y(\Lambda_s r_{ij})\right],
\end{aligned} \tag{4}$$

where $\boldsymbol{\lambda}^a$ represents the $SU(3)$ Gell-Mann matrices that act on the flavor wave functions of the quark system. The Yukawa function $Y(x)$ is explicitly defined as $Y(x)=\dfrac{\mathrm{e}^{-x}}{x}$, where Λ_χ represents the cut-off parameter, and $\dfrac{g_{\rm ch}^2}{4\pi}$ corresponds to the coupling constant between the Goldstone bosons and quarks. The masses of the Goldstone bosons π, K, and η are denoted by m_π, m_η, and m_K, respectively. Meanwhile, the mass of the scalar meson m_σ is related to the pion mass as $m_\sigma^2\approx m_\pi^2+4m_{u,d}^2$.

For confinement potential, we utilize the following quadratic form in this study. Goldman [20] demonstrated that, in a relativistic first-order dynamical system, an interaction energy that increases linearly with the fermion separation has a broad range where a harmonic approximation is applicable for the second-order reduction of the equations of motion. In addition, hadrons are small in size, and within this range, the difference between linear and quadratic confinement potentials is negligible. In addition, this difference can be effectively absorbed by parameters a_c and Δ in the quadratic potential.

$$V_{\rm con}(r_{ij})=\left(-a_c r_{ij}^2-\Delta\right)\boldsymbol{\lambda}_i^c\cdot\boldsymbol{\lambda}_j^c. \tag{5}$$

The one-gluon exchange potential $V_{\rm oge}(r_{ij})$ can be written as

$$V_{\rm oge}(r_{ij})=\frac{\alpha_s}{4}\boldsymbol{\lambda}_i^c\cdot\boldsymbol{\lambda}_j^c\left[\frac{1}{r_{ij}}-\frac{2}{3m_im_j}\hat{S}_i\cdot\hat{S}_j\,\frac{\mathrm{e}^{-r_{ij}/r_0(\mu_{ij})}}{r_{ij}r_0^2(\mu_{ij})}\right], \tag{6}$$

where $\boldsymbol{\lambda}^c$ refers to the $SU(3)$ Gell-Mann matrices acting on the color wave functions of the quark system, r_0 represents a model parameter, α_s represents the coupling constant determined through experimental fitting, and $\hat{S}_i$ represents the spin operator acting on the spin-1/2 wave functions of quarks.

After fitting the ground states of light mesons and baryons, all model parameters are determined, which are collected into Table 1, while the fit results are presented in Table 2.

B. Wave function of the $\Sigma(1/2^-)$ system

We aim to study the $\Sigma(1/2^-)$ system from both the three-quark and five-quark perspectives. Therefore, we

Table 1. Quark model parameters ($m_\pi=0.7$ fm^{-1}, $m_\sigma=3.42$ fm^{-1}, $m_\eta=2.77$ fm^{-1}, and $m_K=2.51$ fm^{-1}). The fourth column corresponds to the first set of parameters while the fifth column corresponds to the second set of parameters.

Quark masses	$m_u=m_d$(MeV)	490	400
	m_s(MeV)	511	550
Goldstone bosons	Λ_π(fm^{-1})	3.5	3.5
	Λ_η(fm^{-1})	2.2	2.2
	Λ_σ(fm^{-1})	7.0	7.0
	Λ_{a_0}(fm^{-1})	2.5	2.5
	Λ_{f_0}(fm^{-1})	1.2	1.2
	$g_{ch}^2/(4\pi)$	0.54	0.54
	$\theta_p(^\circ)$	−15	−15
Confinement	a_c (MeV·fm^{-2})	98	120
	$\Delta_{qq/q\bar{q}}$(MeV)	–91.1/–10.1	–92.4/–20.1
	$\Delta_{qs/q\bar{s}}$(MeV)	–58.0/–10.0	–60.4/–20.0
	$\Delta_{s\bar{s}}$(MeV)	18.1	–18.1
OGE	$\alpha_{qq/q\bar{q}}$	0.69/1.34	0.61/1.31
	$\alpha_{qs/q\bar{s}}$	0.90/1.15	0.95/1.16
	$\alpha_{s\bar{s}}$	0.91	0.91
	$\hat{r}_0$(MeV)	80.9	85.1

Table 2. Results of the hadron spectrum calculation. QM.1 and QM.2 represent the mass of the states under two different sets of parameters.

IJ^P	state	QM.1	QM.2	PDG [5]
10^-	π	143	147	139
00^-	η	599	623	547
11^-	ρ	786	720	770
01^-	ω	800	733	782
$\frac{1}{2}0^-$	K	495	512	495
$\frac{1}{2}1^-$	K^*	915	893	892
00^-	η'	804	828	957
01^-	ϕ	1029	1052	1020
$\frac{1}{2}\frac{1}{2}^+$	N	939	939	939
$\frac{3}{2}\frac{1}{2}^+$	Δ	1271	1297	1232
$0\frac{1}{2}^+$	Λ	1071	1063	1116
$1\frac{1}{2}^+$	Σ	1215	1224	1226
$1\frac{3}{2}^+$	Σ^*	1345	1363	1384
$1\frac{1}{2}^+$	$\Sigma(\frac{1}{2}^-)$	1782	1826	1750
$1\frac{1}{2}^+$	$\Sigma^*(\frac{1}{2}^-)$	1829	1889	1900
$\frac{1}{2}\frac{1}{2}^+$	Ξ	1369	1363	1318
$\frac{1}{2}\frac{1}{2}^+$	Ξ^*	1479	1491	1553
$\frac{3}{2}\frac{1}{2}^+$	Ω	1671	1694	1672

present our constructions for the wave functions (Ψ^P and Ψ^B) of $\Sigma(1/2^-)$. Ψ^B represents the three-quark structure wave function, while Ψ^P represents the five-quark structure wave function. The total wave function Ψ is the tensor product of the color part ξ^l, flavor part ψ^k, orbital part ϕ^i, and spin part χ^j.

$$\Psi^{B_{ijkl}}_{J,m_J}(r) = \mathcal{A}_3\left[\phi^{B_i}_l \chi^{B_j}\right]_{J,m_J} \psi^{B_k}_{I,m_I} \xi^{B_l}, \tag{7}$$

$$\Psi^{P_{ijkl}}_{J,m_J}(r) = \mathcal{A}_5\left[\phi^{P_i}_l \chi^{P_j}\right]_{J,m_J} \psi^{P_k}_{I,m_I} \xi^{P_l}, \tag{8}$$

where $\mathcal{A}_3$ and $\mathcal{A}_5$ represent the antisymmetrization operators for the three-quark and five-quark wave functions, respectively.

For the orbital wave function ϕ_{nlm} (which we will denote as ϕ^i_l for convenience), we adopt the GEM [21] for expansion. In the GEM framework, the wave function with principal quantum number n, orbital quantum number l, and magnetic quantum number m can be expressed as

$$\phi_{nlm}(r) = N_{nl} r^l \mathrm{e}^{-\nu_n r^2} Y_{lm}(r), \tag{9}$$

with N_{nl} being the normalization constants as

$$N_{nl} = \left[\frac{2^{l+2}(2\nu_n)^{l+\frac{3}{2}}}{\sqrt{\pi}(2l+1)}\right]^{\frac{1}{2}}. \tag{10}$$

For the three-quark system, there are two relative motions, whereas for the five-quark system, there are four relative motions. We denote the total orbital wave function for the three-quark system as $\phi^B_{L,m_L}(r)$, and the total orbital wave function for the five-quark system as $\phi^P_{L,m_L}(r)$. These wave functions can be written as

$$\phi^{B_1}_{L,m_L}(r) = \phi_{l_{12}}(r_{12})\phi_{l_3}(r_3), \tag{11}$$

$$\phi^{P_1}_{L,m_L}(r) = \phi_{l_{12}}(r_{12})\phi_{l_3}(r_3)\phi_{l_{45}}(r_{45})\phi_{l_{123,45}}(R). \tag{12}$$

The subscripts in the wave functions represent the relative motion between specific quarks. For example, subscript 12 refers to the relative motion between quarks 1 and 2, and 123,45 refers to the relative motion between quarks 1, 2, and 3 with respect to quarks 4 and 5.

The spin wave function of the three-quark system can be of two possible spin configurations: $S = 1/2$ and $S = 3/2$. For $S = 1/2$, it can be obtained by coupling the spin $S_1 = 1/2$ of quark 1 with the spin $S_2 = 1/2$ of quark 2, which results in the intermediate spin $S_{12} = 0, 1$. Then, this is coupled with the spin $S_3 = 1/2$ of the third quark to obtain the total spin $S = 1/2$. We denote the former case as $\chi^{B_1}_{\frac{1}{2}}$ and the latter as $\chi^{B_2}_{\frac{1}{2}}$. The $S = 3/2$ configuration is denoted as $\chi^{B_3}_{\frac{3}{2}}$.

$$\chi^{B_1}_{\frac{1}{2},\frac{1}{2}} = \frac{1}{\sqrt{2}}(\alpha\beta\alpha - \beta\alpha\alpha), \tag{13}$$

$$\chi^{B_1}_{\frac{1}{2},-\frac{1}{2}} = \frac{1}{\sqrt{2}}(\alpha\beta\beta - \beta\alpha\beta), \tag{14}$$

$$\chi^{B_2}_{\frac{1}{2},\frac{1}{2}} = \frac{1}{\sqrt{6}}(2\alpha\alpha\beta - \alpha\beta\alpha - \beta\alpha\alpha), \tag{15}$$

$$\chi^{B_2}_{\frac{1}{2},-\frac{1}{2}} = \frac{1}{\sqrt{6}}(\alpha\beta\beta + \beta\alpha\beta - 2\beta\beta\alpha), \tag{16}$$

$$\chi^{B_3}_{\frac{3}{2},\frac{3}{2}} = \alpha\alpha\alpha, \tag{17}$$

$$\chi^{B_3}_{\frac{3}{2},\frac{1}{2}} = \frac{1}{\sqrt{3}}(\alpha\alpha\beta + \alpha\beta\alpha + \beta\alpha\alpha), \tag{18}$$

$$\chi^{B_3}_{\frac{3}{2},-\frac{1}{2}} = \frac{1}{\sqrt{3}}(\alpha\beta\beta+\beta\alpha\beta+\beta\beta\alpha), \tag{19}$$

$$\chi^{B_3}_{\frac{3}{2},-\frac{3}{2}} = \beta\beta\beta. \tag{20}$$

The spin wave function of the five-quark system can be considered as the coupling of the spin of a three-quark subsystem and spin of a quark-antiquark pair. Given that $J^P = 1/2^-$, this can be obtained by coupling the following spin configurations: $\frac{1}{2}\otimes 0$, $\frac{1}{2}\otimes 1$, and $\frac{3}{2}\otimes 1$. According to the previous discussion, when the spin of the three-quark system is $1/2$, there are two possible configurations. Therefore, we can obtain five total spin $1/2$ wave functions. These are denoted sequentially as $\chi^{P_1}_{\frac{1}{2}}$, $\chi^{P_2}_{\frac{1}{2}}$, $\chi^{P_3}_{\frac{1}{2}}$, $\chi^{P_4}_{\frac{1}{2}}$, and $\chi^{P_5}_{\frac{1}{2}}$.

$$\begin{aligned}
\chi^{P_1}_{\frac{1}{2},\frac{1}{2}} &= \frac{1}{\sqrt{2}}(\alpha\beta\alpha-\beta\alpha\alpha)\times\frac{1}{\sqrt{2}}(\alpha\beta-\beta\alpha),\\
\chi^{P_2}_{\frac{1}{2},\frac{1}{2}} &= \frac{1}{\sqrt{6}}(2\alpha\alpha\beta-\alpha\beta\alpha-\beta\alpha\alpha)\times\frac{1}{\sqrt{2}}(\alpha\beta-\beta\alpha),\\
\chi^{P_3}_{\frac{1}{2},\frac{1}{2}} &= \frac{1}{\sqrt{12}}(\alpha\beta\alpha\alpha\beta+\alpha\beta\alpha\beta\alpha-\beta\alpha\alpha\alpha\beta-\beta\alpha\alpha\beta\alpha\\
&\quad -2\alpha\beta\beta\alpha\alpha-2\beta\alpha\beta\alpha\alpha),\\
\chi^{P_4}_{\frac{1}{2},\frac{1}{2}} &= \frac{1}{\sqrt{36}}(2\alpha\alpha\beta\alpha\beta+2\alpha\alpha\beta\beta\alpha-\alpha\beta\alpha\alpha\beta-\alpha\beta\alpha\beta\alpha\\
&\quad -\beta\alpha\alpha\alpha\beta-\beta\alpha\alpha\beta\alpha-2\alpha\beta\beta\alpha\alpha\\
&\quad +2\beta\alpha\beta\alpha\alpha-4\beta\beta\alpha\alpha\alpha),\\
\chi^{P_5}_{\frac{1}{2},\frac{1}{2}} &= \frac{1}{\sqrt{18}}(\alpha\beta\beta\alpha\alpha+\beta\alpha\beta\alpha\alpha+\beta\beta\alpha\alpha\alpha-\alpha\alpha\beta\alpha\beta\\
&\quad -\alpha\alpha\beta\beta\alpha-\alpha\beta\alpha\alpha\beta-\alpha\beta\alpha\beta\alpha-\beta\alpha\alpha\alpha\beta\\
&\quad -\beta\alpha\alpha\beta\alpha+3\alpha\alpha\alpha\beta\beta).
\end{aligned}$$

The isospin of the $\Sigma(1/2^-)$ system is 1. In the three-quark framework, its flavor wave function $\psi^{B_1}_{I=1}$ can be expressed as

$$\psi^{B_1}_{I=1} = \frac{1}{\sqrt{2}}(uds+dus). \tag{21}$$

In the five-quark framework, it has two possible flavor combinations: $qqq-\bar{q}s$ and $qqs-\bar{q}q$. In the first flavor structure $qqq-\bar{q}s$, the total isospin $I=1$ coupling scheme is $\frac{1}{2}\otimes\frac{1}{2}$ and $\frac{3}{2}\otimes\frac{1}{2}$. Since $\frac{1}{2}$ can be obtained by coupling $0\otimes\frac{1}{2}$ or $1\otimes\frac{1}{2}$, we can obtain three total isospin wave functions. These are denoted as $\psi^{P_1}_{I=1}$, $\psi^{P_2}_{I=1}$, and $\psi^{P_3}_{I=1}$.

$$\psi^{P_1}_{I=1} = \frac{1}{\sqrt{2}}(ud u\bar{d}s-duu\bar{d}s), \tag{22}$$

$$\psi^{P_2}_{I=1} = \frac{1}{\sqrt{6}}(2uud\bar{d}s-ud u\bar{d}s-duu\bar{d}s), \tag{23}$$

$$\psi^{P_3}_{I=1} = \frac{1}{\sqrt{12}}(uud\bar{d}s+ud u\bar{d}s+duu\bar{d}s+3uuu\bar{u}s). \tag{24}$$

In the second flavor structure $qqs-\bar{q}q$, the total isospin $I=1$ coupling schemes are $0\otimes1$, $1\otimes0$, and $1\otimes1$. These are denoted as $\psi^{P_4}_{I=1}$, $\psi^{P_5}_{I=1}$, and $\psi^{P_6}_{I=1}$.

$$\psi^{P_4}_{I=1} = \frac{1}{\sqrt{2}}(uds\bar{d}u-dus\bar{d}u), \tag{25}$$

$$\psi^{P_5}_{I=1} = \frac{1}{\sqrt{2}}(uus\bar{u}u+uus\bar{d}d), \tag{26}$$

$$\psi^{P_6}_{I=1} = \frac{1}{\sqrt{4}}(-uds\bar{d}u-dus\bar{d}u-uus\bar{d}u+uus\bar{d}d). \tag{27}$$

For the color wave function in a three-quark system, it must be in a color-neutral state. Hence, it is expressed as

$$\xi^B = \frac{1}{\sqrt{6}}(rgb-grb+gbr-brg+bgr). \tag{28}$$

For a five-quark system, the color wave function can be viewed as the combination of the three-quark and two-quark color wave functions when considering a molecular state configuration. This can be obtained by coupling two color singlet states, which is represented by ξ^{P_1} and written as

$$\begin{aligned}
\xi^{P_1} &= \frac{1}{\sqrt{6}}(rgb-rbg+gbr-grb+brg-bgr)\\
&\quad\times\frac{1}{\sqrt{3}}\left(\bar{r}r+\bar{g}g+\bar{b}b\right).
\end{aligned} \tag{29}$$

C. Complex-scaling method

The complex-scaling method introduced in Refs. [22, 23] is a robust technique for identifying resonant states. This method involves replacing the spatial coordinates $\vec{r}$ in the Hamiltonian H with $\vec{r}e^{i\theta}$, where θ represents a complex scaling factor. Both the energy and decay width (lifetime) of the resonance can be simultaneously determined by solving the Schrodinger equation in the complex plane.

In the complex-scaling framework, the real part of the complex energy M is plotted along the horizontal axis, while the half-width $\Gamma/2$ is plotted along the vertical axis. The system shows different characteristic behaviors as

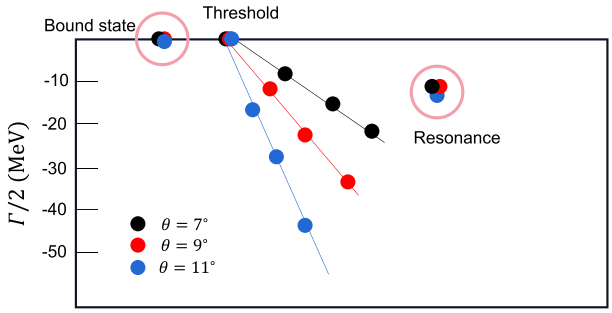

Fig. 2. (color online) Schematic of the complex energy distribution.

the scaling angle θ varies. The method enables the simultaneous study of bound states, resonances, and scattering states, which are shown in Fig. 2. Their behaviors as θ changes are as follows:

• **Bound states:** For bound states, the corresponding points converge to the real energy axis. The position of these points on the real axis directly gives the mass of the bound state.

• **Scattering states:** Points corresponding to scattering states lie along the scattering line, where θ is constant. The scattering spectrum is continuous, and therefore, an infinite number of points would theoretically lie along this line. To avoid clutter, only a few representative points are shown to illustrate the general trend within the energy range.

• **Resonances:** Resonance points do not lie on the scattering continuum (scattering line) but stay fixed as θ changes. The vertical position of these points represents the half-width $\Gamma/2$. The resonance width is a result of coupling to open scattering channels, and hence, no width is predicted for purely three-quark or two-quark systems.

A key advantage of the complex-scaling method is that transforming the system into the complex coordinate plane significantly enhances the analysis of resonant states. This makes it a powerful tool for exploring resonance phenomena in systems governed by strong interactions.

III. RESULTS AND DISCUSSIONS

We first explore the possible internal quark configurations of the $\Sigma(1/2^-)$ resonance within the three-quark framework. Then, we perform bound-state calculations within the five-quark model to identify physical channels exhibiting attractive interactions, which may indicate the formation of resonance states. Within the complex-scaling framework, these resonance candidates are coupled to all relevant scattering channels to distinguish genuine resonances from unstable ones. All calculations are performed under two different parameter sets to assess the stability of the computed results. In addition, we further perform channel-coupling calculations between each resonance candidate and corresponding open channels to estimate the decay widths of stable resonances and analyze the scattering behavior of unstable ones.

A. Three-quark calculation

Baryon energies obtained from three-quark calculations are listed in Table 2. Under the two parameter sets, the ground states $\Sigma(1/2^+)$ and $\Sigma(3/2^+)$ are in good agreement with experimental observations. Based on this, under the first set of parameters, their respective first excited states are found at 1782 and 1829 MeV, while under the second set of parameters, their respective first excited states are found at 1826 and 1889 MeV, which are consistent with the experimentally observed $\Sigma(1750)$ and $\Sigma(1900)$, respectively. From another perspective, mass differences between the ground states $\Sigma(1/2^+)$, $\Sigma(3/2^+)$ and their excited counterparts $\Sigma(1750)$, $\Sigma(1900)$ are both around 500 MeV. This is comparable to the average mass difference between the $1P$ and $1S$ states of mesons such as $\rho(770)$-$a_1(1260)$ (490 MeV), $K^*(895)$-$K_1(1270)$ (375 MeV), $K(495)$-$K_1(1270)$ (775 MeV), $\eta'(958)$-$f_1(1420)$ (462 MeV), and $\phi(1020)$-$f_1(1420)$ (400 MeV). The average of these values is ~500 MeV.

Therefore, it is reasonable to consider that the experimentally observed $\Sigma(1750)$ and $\Sigma(1900)$ are likely dominated by three-quark components, which is similar to $\Lambda(1670)$ and $\Lambda(1800)$ resonances in the $\Lambda(1/2^-)$ sector. If there exists a one-to-one correspondence between $\Sigma(1/2^-)$ and $\Lambda(1/2^-)$ families, then $\Sigma(1/2^-)$ resonances should exist in the 1.3−1.4 GeV mass region, analogous to the $\Lambda(1405)$ and $\Lambda(1380)$, and it is predominantly composed of five-quark components.

B. Five-quark calculations

1. *Bound-state calculation*

The results for the five-quark system are listed in Table 3. The $\Sigma(1/2^-)$ five-quark system has two possible quark configurations qqq-$\bar{q}s$ and qqs-$\bar{q}q$. In the first quark configuration qqq-$\bar{q}s$, the total isospin $I=1$ coupling occurs in the forms $\frac{1}{2}\otimes\frac{1}{2}$ and $\frac{3}{2}\otimes\frac{1}{2}$. For the total spin $J=1/2$, the coupling schemes are $\frac{1}{2}\otimes 0$, $\frac{1}{2}\otimes 1$, and $\frac{3}{2}\otimes 1$. Quantum combinations corresponding to these are $N\bar{K}$, $N\bar{K}^*$, and $\Delta\bar{K}^*$. In the second quark configuration qqs-$\bar{q}q$, the total isospin $I=1$ coupling can be $0\otimes 1$, $1\otimes 0$, or $1\otimes 1$, whereas the total spin $J=1/2$ coupling includes $\frac{1}{2}\otimes 0$, $\frac{1}{2}\otimes 1$, and $\frac{3}{2}\otimes 1$. The corresponding quantum combinations for these are $\Lambda\pi$, $\Lambda\rho$, $\Sigma\pi$, $\Sigma\rho$, $\Sigma\eta$, $\Sigma\omega$, $\Sigma^*\omega$, and $\Sigma^*\rho$.

Therefore, in our calculations, we considered a total

Table 3. Energies of the $\Sigma^*(1/2^-)$ system. i,j,k,l represent the index of orbit, flavor, spin, and color wave functions, respectively. $E_{\rm th}$, $E_{\rm sc}$, and $E_{\rm mix}$ represent the threshold of the corresponding channel, energy of every single channel, and lowest energy of the system by coupling all channels, respectively. (unit: MeV)

$\Psi^{P_{ijkl}}_{\frac{1}{2},\frac{1}{2}}$	Channel	$E_{\rm th1}$	$E_{\rm sc1}$	$B.E.$	$E_{\rm mix1}$	$E_{\rm th2}$	$E_{\rm sc2}$	$B.E.$	$E_{\rm mix2}$
$\Psi^{P_{1111}}_{\frac{1}{2},\frac{1}{2}}/\Psi^{P_{1261}}_{\frac{1}{2},\frac{1}{2}}$	$N\bar{K}$	1435.3	1417.4	17.9	1215.6	1452.6	1443.1	9.5	1214.0
$\Psi^{P_{1221}}_{\frac{1}{2},\frac{1}{2}}/\Psi^{P_{1461}}_{\frac{1}{2},\frac{1}{2}}$	$N\bar{K}^*$	1854.3	1839.7	14.6		1834.2	1826.4	7.8	
$\Psi^{P_{1351}}_{\frac{1}{2},\frac{1}{2}}$	$\Delta\bar{K}^*$	2186.4	2188.4	ub		2191.1	2193.5	ub	
$\Psi^{P_{1621}}_{\frac{1}{2},\frac{1}{2}}$	$\Sigma\pi$	1358.5	1348.5	10.0		1372.8	1366.6	6.2	
$\Psi^{P_{1641}}_{\frac{1}{2},\frac{1}{2}}$	$\Sigma\rho$	2001.8	1995.1	6.7		1958.6	1957.9	0.7	
$\Psi^{P_{1651}}_{\frac{1}{2},\frac{1}{2}}$	$\Sigma^*\rho$	2132.6	2130.3	2.3		2096.9	2097.8	ub	
$\Psi^{P_{1411}}_{\frac{1}{2},\frac{1}{2}}$	$\Lambda\pi$	1214.9	1216.8	ub		1211.5	1214.2	ub	
$\Psi^{P_{1431}}_{\frac{1}{2},\frac{1}{2}}$	$\Lambda\rho$	1858.2	1859.5	ub		1797.3	1799.6	ub	
$\Psi^{P_{1521}}_{\frac{1}{2},\frac{1}{2}}$	$\Sigma\eta$	1814.8	1816.2	ub		1848.8	1851.3	ub	
$\Psi^{P_{1541}}_{\frac{1}{2},\frac{1}{2}}$	$\Sigma\omega$	2015.3	2016.1	ub		1945.8	1948.0	ub	
$\Psi^{P_{1551}}_{\frac{1}{2},\frac{1}{2}}$	$\Sigma^*\omega$	2146.1	2144.9	1.2		2084.8	2085.3	ub	

of 11 physical channels. Under the first set of parameters, the energy distribution of these channels spans the range from 1.2 to 2.1 GeV. Among them, we identified six bound states, which are $N\bar{K}$, $N\bar{K}^*$, $\Sigma\pi$, $\Sigma\rho$, $\Sigma^*\omega$, and $\Sigma^*\rho$. The binding energies of the first three channels, $N\bar{K}$, $N\bar{K}^*$, and $\Sigma\pi$, are all greater than 10 MeV, while the binding energies of the remaining three channels are only a few mega-electron volt. This implies that the first three channels, namely, $N\bar{K}$, $N\bar{K}^*$, and $\Sigma\pi$, are more likely to form stable resonant states. Under the second set of parameters, these states, $N\bar{K}$, $N\bar{K}^*$, and $\Sigma\pi$, remain stable and are still bound states, with binding energies around $6-9$ MeV. In addition, $\Sigma\rho$ has a binding energy of 6.7 MeV under the first set of parameters, but only 0.7 MeV under the second set, which indicates that it is not very stable. Therefore, under both parameter sets, $N\bar{K}$, $N\bar{K}^*$, $\Sigma\rho$, and $\Sigma\pi$ are bound states, while under the first set of parameters, $\Sigma^*\omega$ and $\Sigma^*\rho$, though also shallow bound states with binding energies of $1-2$ MeV, do not survive under the second set of parameters.

We systematically studied the contributions of each Hamiltonian term to the binding energy (threshold minus calculated value) for these six states to understand this discrepancy, and the results are listed in Table 4. We ob-

Table 4. Contributions of all potentials to the binding energy (unit: MeV) in $\Sigma(1/2^-)$ five-quark system, where Q.M.1 and Q.M.2 represent the calculation results under two different sets of parameters.

		kinetic	con	oge	π	η	σ	a_0	f_0
$N\bar{K}$	Q.M.1	90.0	−5.6	−12.0	−2.7	−1.1	−78.1	−6.6	−3.0
	Q.M.2	64.2	−4.6	−6.2	−2.1	−0.0	−54.0	−4.6	−2.3
$N\bar{K}^*$	Q.M.1	76.9	−6.1	−8.3	−2.1	−0.1	−66.7	−5.7	−2.7
	Q.M.2	55.5	−4.5	−4.2	−1.7	−0.0	−46.7	−4.0	−2.1
$\Sigma\pi$	Q.M.1	64.9	−4.0	−7.2	2.5	−0.1	−62.5	−3.6	−0.0
	Q.M.2	31.1	−1.8	−3.3	1.7	−0.0	−28.8	−1.7	−0.0
$\Sigma\rho$	Q.M.1	50.3	−3.5	−5.2	3.5	−0.1	−48.1	−3.5	−0.1
	Q.M.2	20.1	−1.3	−1.5	2.9	−0.0	−18.5	−1.1	−0.0
$\Sigma^*\rho$	Q.M.1	27.6	−2.2	−2.5	0.0	0.3	−28.0	−0.0	−0.0
	Q.M.2	9.6	−0.6	−0.5	1.0	0.0	−8.7	−0.0	−0.0
$\Sigma^*\omega$	Q.M.1	20.5	−1.6	−0.3	1.1	0.2	−21.0	0.1	0.0
	Q.M.2	8.0	−0.5	−0.1	0.1	0.0	−7.0	0.0	0.0

serve that the kinetic energy predominantly contributes to repulsive forces, while the attraction comes from the σ-meson exchange, one-gluon-exchange, and a_0-meson exchange with the σ-meson exchange playing a dominant role. The kinetic and potential energies compete with each other; the quarks are brought closer together with an increase in attractive potential, thereby leading to an increase in the repulsive kinetic energy. Compared to the second set, binding energies under the first set are generally larger, which results in larger kinetic energy and stronger attractive potential contributions. Under the second set of parameters, the σ-meson exchange for the $\Sigma^*\omega$ and $\Sigma^*\rho$ states provides insufficient attraction (less than 10 MeV), which canont overcome the repulsive kinetic energy and prevent these states from forming bound states.

2. *Resonance-state calculation*

We aim to use the effects of channel coupling to check if the resonance candidates obtained from the bound state calculation survive in the channel coupling framework. Based on the bound state calculations under the two parameter sets, we identified three relatively stable bound states, namely $N\bar{K}$, $N\bar{K}^*$, and $\Sigma\pi$, one less stable bound state, $\Sigma\rho$, and two more controversial bound states, $\Sigma^*\omega$ and $\Sigma^*\rho$. Under both parameter sets, we perform a complete channel coupling calculation using the complex-scaling method for all channels to search for stable resonance states. Then, we perform channel coupling calculations between the bound states identified in the previous calculations and corresponding threshold channels to obtain the decay widths of resonance states, and we investigate the channel coupling mechanisms (*i.e.*, the reasons why unstable bound states transform into scattering states). The energy range of the five-quark system under investigation is between 1.2 and 2.1 GeV. The resonance-state calculation is performed to verify if the resonance candidates identified in the bound state calculation correspond to genuine resonances. Therefore, in Figs. 3 and 4, we present the energy range from 1.2 to 2.2 GeV.

As shown in Fig. 3, we obtained three stable resonance states, namely $R(1302)$, $R(1395)$, and $R(1830)$ (we use "R(Energy)" to denote Resonance.). We performed a component analysis of these three resonance states, and the results (see Table 6) show that $R(1302)$ and $R(1395)$ include $N\bar{K}$-$\Sigma\pi$ coupling. $R(1302)$ has a dominant $\Sigma\pi$ component (about 53.1%), while $R(1395)$ has a dominant $N\bar{K}$ component (about 73.3%). $R(1830)$ has a main component of $N\bar{K}^*$ (about 51.6%) and an important $\Sigma\eta$ component (about 33.4%). This implies that the $N\bar{K}^*$-$\Sigma\eta$ coupling is significant; however, there is no attraction between $\Sigma\eta$. Therefore, even though the $N\bar{K}^*$-$\Sigma\eta$ coupling is strong, it still cannot form a resonance state dominated by $\Sigma\eta$. Thus, their main components are $\Sigma\pi$, $N\bar{K}$, and $N\bar{K}^*$, respectively. Meanwhile, another shallow bound state $\Sigma^*\rho$, and two controversial bound states, $\Sigma^*\omega$ and $\Sigma^*\rho$, obtained in the previous bound-state calculations did not survive in the channel coupling calculation and became scattering states. This conclusion is corroborated by the results under the second set of parameters, as shown in Fig. 4, where $R(1302)$, $R(1395)$, and $R(1830)$ are stable resonance states. In our calculations, the energies of the predicted $R(1302)$ and $R(1395)$ are very close to each other, which correspond to the two-pole structure observed experimentally in the $\Lambda(1/2^-)$ system, namely $\Lambda(1380)$ and $\Lambda(1405)$. The $\Lambda(1/2^-)$ and $\Sigma(1/2^-)$ systems differ only by isospin, and therefore, the prediction of $R(1302)$ and $R(1395)$ is highly credible. The energy of $R(1830)$ lies between $\Sigma(1750)$ and $\Sigma(1900)$, which suggests that $R(1830)$ is one of the five-quark candidates for these states.

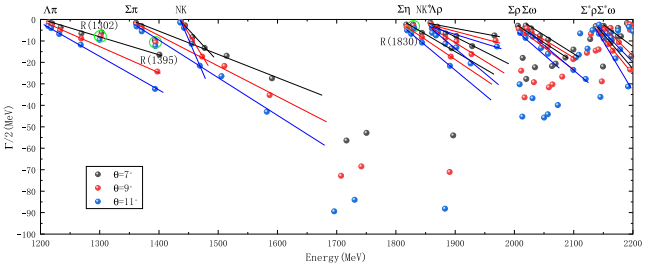

Fig. 3. (color online) Complex-scaling results for the $\Sigma(1/2^-)$ five-quark system in the 1200−2200 MeV range for the first set of parameters.

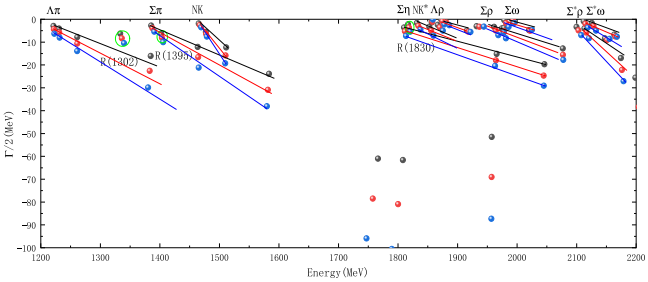

Fig. 4. (color online) Complex-scaling results for the $\Sigma(1/2^-)$ five-quark system in the 1200−2200 MeV rangefor the second set of parameters.

We performed channel coupling calculations with all possible decay channels to obtain the decay widths for the genuine resonance states and investigate why unstable resonances such as $\Sigma\rho$, $\Sigma^*\omega$, and $\Sigma^*\rho$ decay into scattering states. The decay widths are shown in Fig. 5 and listed in Table 5. The results of the unstable resonances coupling with decay channels and transitioning into scattering states are shown in Fig. 6. The resonance states obtained from both parameter sets are consistent in our calculations, and therefore, the decay widths are only provided for the first parameter set. According to our calculations, in Fig. 5, the decay width of $R(1302)$ to $\Lambda\pi$ is

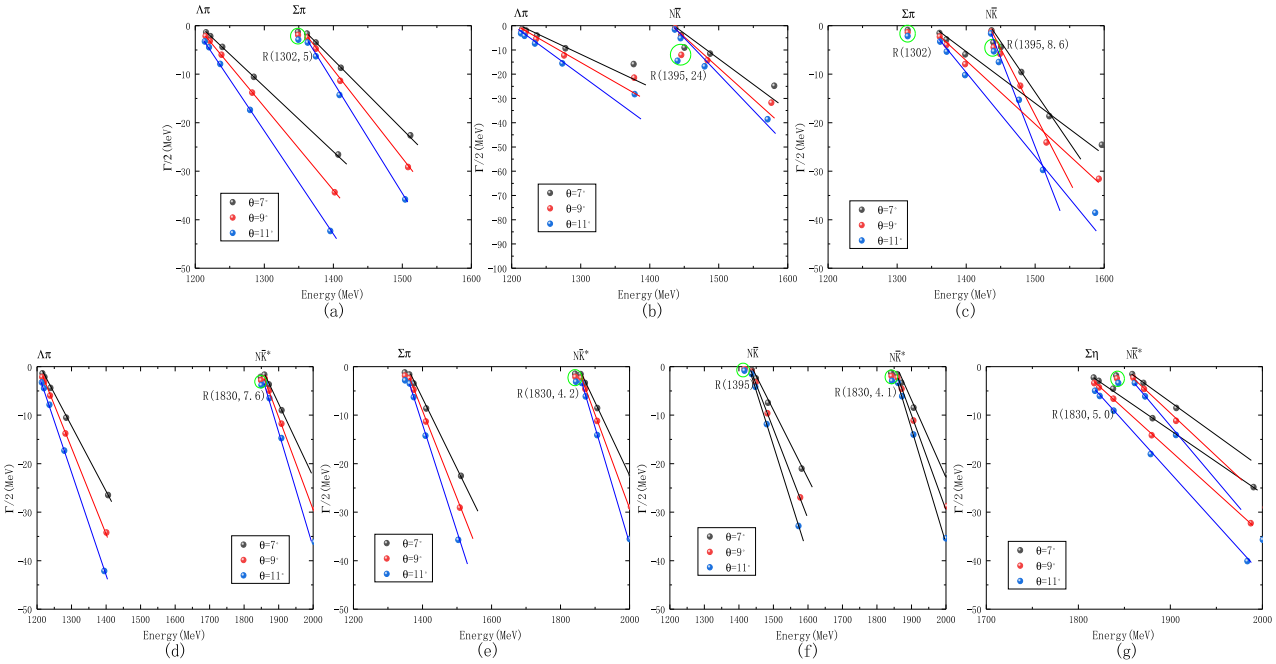

Fig. 5. (color online) Calculated decay widths of resonance states in the Σ(1/2⁻) five-quark system.(a)$\Sigma\pi \to \Lambda\pi$. (b)$N\bar{K} \to \Lambda\pi$. (c)$N\bar{K} \to \Sigma\pi$. (d)$N\bar{K}^* \to \Lambda\pi$. (e)$N\bar{K}^* \to \Sigma\pi$. (f)$N\bar{K}^* \to N\bar{K}$. (g)$N\bar{K}^* \to \Sigma\eta$.

Table 5. Various decay channels and corresponding decay widths of obtained resonances. (unit: MeV)

Decay channels	$R(1302)$	P	$R(1395)$	P	$R(1830)$	P
$\Lambda\pi$	5.0	100%	24.0	74%	7.6	37%
$\Sigma\pi$	…	…	8.6	26%	4.2	20%
$N\bar{K}$	…	…	…	…	4.1	19%
$\Sigma\eta$	…	…	…	…	5.0	24%
Total	5.0		32.6		20.9	

5.0 MeV, and because this is the only decay channel, the total width is 5.0 MeV. For $R(1395)$, the decay widths to $\Lambda\pi$ and $\Sigma\pi$ are 24.0 and 8.6 MeV, respectively, yielding a total width of 32.6 MeV. For $R(1830)$, the decay widths to $\Lambda\pi$, $\Sigma\pi$, $N\bar{K}$, and $\Sigma\eta$ are 7.6, 4.2, 4.1, and 5.0 MeV, respectively, thereby resulting in a total width of 20.9 MeV. Considering that the experimental widths of Σ(1750) and Σ(1900) are both over 100 MeV from the perspective of decay widths, $R(1830)$ may require additional three-quark components to better explain the experimental Σ(1750) and Σ(1900) states because its width in our calculation is only 20.9 MeV. Therefore, we propose that the experimental Σ(1750) and Σ(1900) are likely to be mixed states, which contains components of both the three-quark Σ(1/2⁻) and five-quark $N\bar{K}^*$ states. Finally, based on the percentage of their decay widths, as shown in Table 5, $R(1302)$ and $R(1395)$ predominantly decay into $\Lambda\pi$ (with more than 70%), while $R(1830)$ has a more complex decay pattern with both $\Lambda\pi$ and $\Sigma\eta$ playing significant roles. According to Fig. 6, the $\Sigma\rho$ state survives only when coupled with the $\Sigma\eta$ and $N\bar{K}^*$ channels, and it rapidly decays into the $\Lambda\pi$, $\Sigma\pi$, $N\bar{K}$, and $\Lambda\rho$ channels. In contrast, the two more controversial resonance candidates, $\Sigma^*\omega$ and $\Sigma^*\rho$, do not survive in any of the coupled decay channels. The reason why $\Sigma\rho$, $\Sigma^*\omega$, and $\Sigma^*\rho$ fail to form genuine resonance states is that their binding energies are too small, and this leads them to transition into scattering states once coupled with most decay channels.

IV. SUMMARY

Within the framework of the chiral quark model, we systematically studied the Σ(1/2⁻) system from the three-quark and five-quark perspectives under two different parameter sets by employing the GEM.

From the three-quark calculations, we obtained two Σ(1/2⁻) states with energies of ~1.75 and 1.82 GeV for the first parameter set, and 1.83 and 1.89 GeV for the second parameter set. These results are in good agreement with the experimentally observed Σ(1750) and Σ(1900), respectively, while simultaneously reproducing the ground states Σ(1/2⁺) and Σ(3/2⁺) with good accuracy. In addition, the energy gap between these excited and ground states is roughly 500 MeV, which is consistent with the typical mass difference between the $1P$ and $1S$ states in light meson systems such as η, ρ, ω, K, and K^*. This observation further supports the interpretation that Σ(1750) and Σ(1900) possess substantial three-quark components.

In the bound-state calculations within the five-quark framework, we obtained three stable bound states: $\Sigma\pi$,

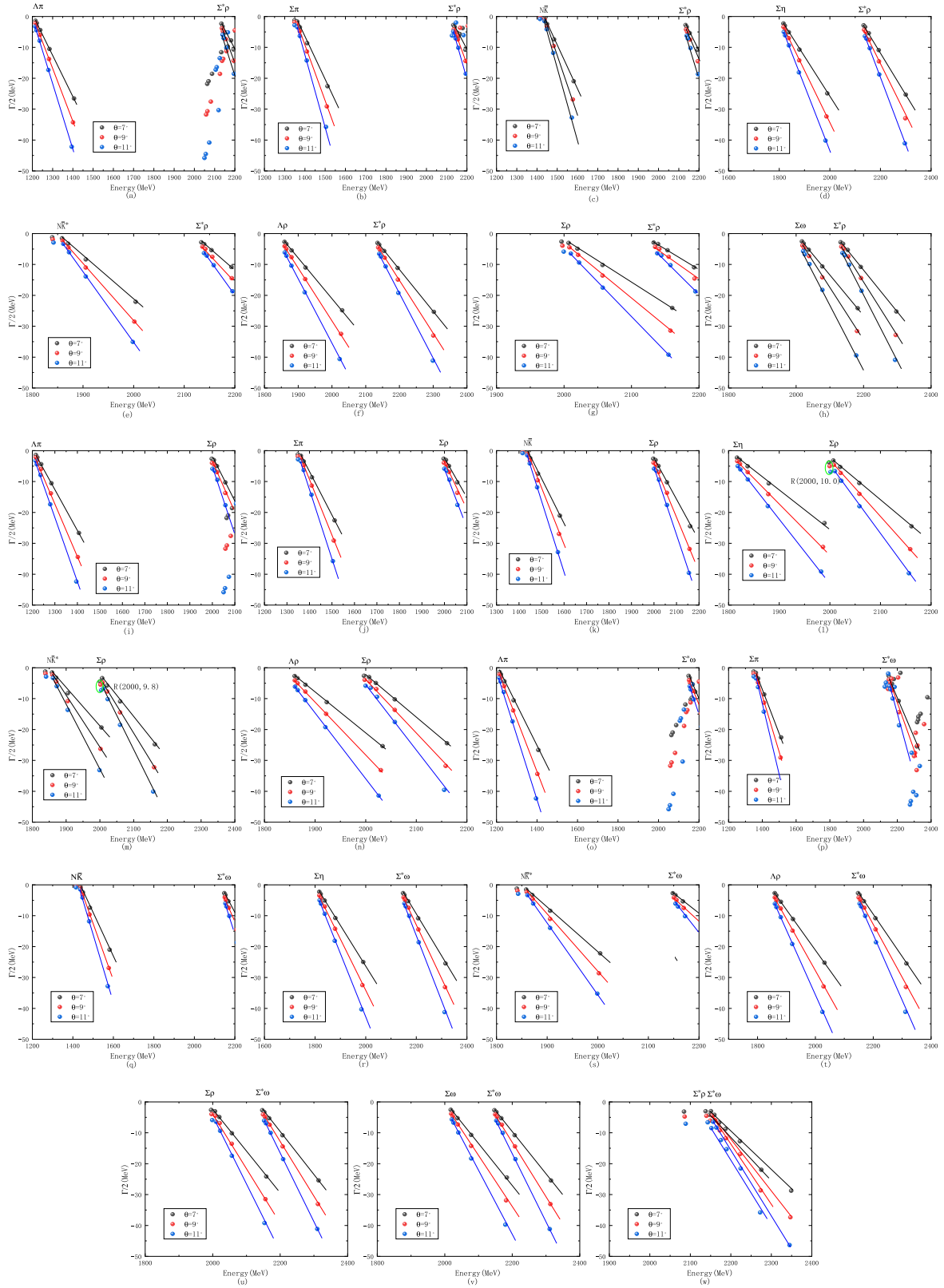

Fig. 6. (color online) Channel-coupling effects transforming some unstable resonances into scattering states in the $\Sigma(1/2^-)$ five-quark system. (a)$\Sigma^*\rho \to \Lambda\pi$.(b)$\Sigma^*\rho \to \Sigma\pi$. (c)$\Sigma^*\rho \to N\bar{K}$. (d)$\Sigma^*\rho \to \Sigma\eta$. (e)$\Sigma^*\rho \to N\bar{K}^*$. (f)$\Sigma^*\rho \to \Lambda\rho$. (g)$\Sigma^*\rho \to \Sigma\rho$. (h)$\Sigma^*\rho \to \Sigma\omega$. (i)$\Sigma\rho \to \Lambda\pi$. (j)$\Sigma\rho \to \Sigma\pi$. (k)$\Sigma\rho \to N\bar{K}$. (l)$\Sigma\rho \to \Sigma\eta$. (m)$\Sigma\rho \to N\bar{K}^*$. (n)$\Sigma\rho \to \Lambda\rho$. (o)$\Sigma^*\omega \to \Lambda\pi$. (p)$\Sigma^*\omega \to \Sigma\pi$. (q)$\Sigma^*\omega \to N\bar{K}$. (r)$\Sigma^*\omega \to \Sigma\eta$. (s)$\Sigma^*\omega \to N\bar{K}^*$. (t)$\Sigma^*\omega \to \Lambda\rho$. (u)$\Sigma^*\omega \to \Sigma\rho$. (v)$\Sigma^*\omega \to \Sigma\omega$. (w)$\Sigma^*\omega \to \Sigma^*\rho$.

Table 6. Main components of the three stable resonance states.

	$N\bar{K}$	$N\bar{K}^*$	$\Delta\bar{K}^*$	$\Sigma\pi$	$\Sigma\rho$	$\Sigma^*\rho$	$\Lambda\pi$	$\Lambda\rho$	$\Sigma\eta$	$\Sigma\omega$	$\Sigma^*\omega$
$R(1302)$	15.5%	0.1%	0.0%	53.1%	0.1%	0.0%	31.0%	0.1%	0.1%	0.0%	0.0%
$R(1395)$	73.3%	0.1%	0.0%	26.1%	0.1%	0.0%	0.9%	0.1%	0.0%	0.0%	0.0%
$R(1830)$	1.5%	51.6%	0.0%	3.9%	0.1%	0.0%	4.5%	5.1%	33.4%	0.0%	0.0%

$N\bar{K}$, and $N\bar{K}^*$, along with a shallower bound state $\Sigma\rho$ and two controversial bound states $\Sigma^*\rho$ and $\Sigma^*\omega$. Our calculations show that, under the effect of channel coupling, the three stable bound states $\Sigma\pi$, $N\bar{K}$, and $N\bar{K}^*$ form stable resonance states $R(1302)$, $R(1395)$, and $R(1830)$, while $\Sigma^*\rho$, $\Sigma^*\omega$, and $\Sigma\rho$ all transition into scattering states. Among these, $R(1302)$ and $R(1395)$, with their main components being the $\Sigma\pi$ and $N\bar{K}$ channels, survive the coupling process and remain stable despite being close in energy, thereby yielding a two-pole structure. These predicted two-pole resonances are similar in nature to the well-established $\Lambda(1380)$-$\Lambda(1405)$ system. The main component of $R(1830)$ is $N\bar{K}^*$, which shows good agreement with the masses of $\Sigma(1750)$ and $\Sigma(1900)$. However, its decay width deviates from the experimental data. This suggests that $R(1830)$ requires additional three-quark components to better explain the experimental $\Sigma(1750)$ and $\Sigma(1900)$ states. In future work, we intend to explore this system using an unquenched quark model to further test our hypothesis.

We obtained three resonance states in the $\Sigma(1/2^-)$ system: $R(1302)$, $R(1395)$, and $R(1830)$. Among these, $R(1302)$-$R(1395)$ exhibits a two-pole structure similar to the $\Lambda(1380)$-$\Lambda(1405)$ system, and we strongly recommend experimental efforts to search for these states in the invariant mass spectrum of $\Lambda\pi$. Although the mass of $R(1830)$ agrees well with the experimental $\Sigma(1750)$ and $\Sigma(1900)$, the calculated width is relatively small. This indicates that three-quark mixing effects may be required to better explain the experimental $\Sigma(1750)$ and $\Sigma(1900)$ states.

References

[1] M. Gell-Mann, Phys. Lett. **8**, 214 (1964)
[2] G. Zweig, doi: 10.17181/CERN-TH-401.
[3] Y. Tan and J. Ping, Phys. Rev. D **100**(3), 034022 (2019)
[4] Y. Tan, Z. X. Ma, X. Chen *et al.*, Phys. Rev. D **111**(9), 096018 (2025)
[5] R. L. Workman *et al.* (Particle Data Group), PTEP **2022**, 083C01 (2022)
[6] A. Zhang, Y. R. Liu, P. Z. Huang *et al.*, Chin. Phys. C **29**, 250 (2005)
[7] J. J. Wu, S. Dulat, and B. S. Zou, Phys. Rev. C **81**, 045210 (2010)
[8] J. J. Wu, S. Dulat, and B. S. Zou, Phys. Rev. D **80**, 017503 (2009)
[9] Q. Huang, Z. X. Ma, J. J. Wu *et al.*, Phys. Rev. D **110**(3), 034018 (2024)
[10] E. Wang, L. S. Geng, J. J. Wu *et al.*, Chin. Phys. Lett. **41**(10), 101401 (2024)
[11] K. Wang, Y. F. Wang, B. C. Liu *et al.*, Phys. Rev. D **110**(9), 094017 (2024)
[12] M. Mai and U. G. Meißner, Eur. Phys. J. A **51**(3), 30 (2015)
[13] M. Mai, Eur. Phys. J. ST **230**(6), 1593 (2021)
[14] L. Qin, Y. Tan, X. Hu *et al.*, Phys. Rev. C **103**(1), 015203 (2021)
[15] N. V. Shevchenko, Phys. Rev. C **85**, 034001 (2012)
[16] J. Vijande, F. Fernandez, and A. Valcarce, J. Phys. G **31**, 481 (2005)
[17] Y. Tan, X. Liu, X. Chen *et al.*, Phys. Rev. D **110**(1), 016005 (2024)
[18] Y. Tan, X. Liu, X. Chen *et al.*, Phys. Rev. D **109**(7), 076026 (2024)
[19] Y. Tan, X. Liu, X. Chen *et al.*, Phys. Rev. D **108**(1), 014017 (2023), arXiv: 2210.16250 [hep-ph]
[20] J. T. Goldman and S. Yankielowicz, Phys. Rev. D **12**, 2910 (1975)
[21] E. Hiyama, Y. Kino, and M. Kamimura, Prog. Part. Nucl. Phys. **51**, 223 (2003)
[22] J. Aguilar and J. M. Combes, Commun. Math. Phys. **22**, 269 (1971)
[23] E. Balslev and J. M. Combes, Commun. Math. Phys. **22**, 280 (1971)